Numerical analysis of agricultural emissions impacts on $PM_{2.5}$ in China using a high-resolution ammonia emission inventory

Xiao Han[1,2], Lingyun Zhu[5],Mingxu Liu[4], Yu Song[4] Meigen Zhang[1,2,3],

[1]*State Key Laboratory of Atmospheric Boundary Layer Physics and Atmospheric Chemistry, Institute of Atmospheric Physics, Chinese Academy of Sciences, Beijing 100029, China*

[2]*College of Earth and Planetary Sciences, University of Chinese Academy of Sciences, Beijing 100049, China*

[3]*Center for Excellence in Urban Atmospheric Environment, Institute of Urban Environment, Chinese Academy of Sciences, Xiamen 361021, China*

[4]*State Key Joint Laboratory of Environmental Simulation and Pollution Control, Department of Environmental Science, Peking University, Beijing 100871, China.*

[5]*Shanxi Province Institute of Meteorological Sciences, Taiyuan 030002, China*

Abstract

China is one of the largest agriculture country in the world. The NH_3 emission from agriculture activities are significantly affects the regional air quality and horizontal visibility in China. To reliably estimate the agriculture NH_3 influence, a high-resolution agriculture NH_3 emission inventory compiled on 1km × 1km horizontal resolution was applied for calculating the NH_3 mass burden in China. The key parameter emission factors of this inventory was enhanced by considering many native experiment results, and the activity data of spatial and temporal information were updated by the statistic data in 2015. Not only fertilizer and husbandry, but also farmland ecosystems, livestock waste, crop residue burning, fuel wood combustion, and other NH_3 emission sources were included in this inventory. Furthermore, a source apportionment tool, ISAM (Integrated Source Apportionment Method), coupled with the air quality modeling system RAMS-CMAQ (Regional Atmospheric Modeling System and Community Multiscale Air Quality), was applied to capture the contribution of NH_3 emitted from total agriculture (Tagr) in China. The aerosol mass concentration in 2015 was simulated and the results showed that the high mass concentration of NH_3 which exceeded 10 μg m^{-3} mainly appeared in the North China Plain (NCP), Central China (CNC), Yangtz River Delta (YRD), and Sichan Basin (SCB), and the annually average contribution of Tagr NH_3 to $PM_{2.5}$ mass burden was 14-22% in China. Specific to the $PM_{2.5}$ components, Tagr NH_3 provided major contribution to the ammonium formation (87.6%), but tiny contribution to the sulfate (2.2%). In addition, several brute-force sensitive tests were conducted to estimate the impact of Tagr NH_3 emission reduction on $PM_{2.5}$ mass burden. Compared with the result of ISAM, it was found that even though the Tagr NH_3 only provided 10.1% contribution to nitrate under current emission scenario, the reduction of nitrate could reach 95.8% upon removal of the Tagr NH_3 emission. The main reason of this deviation should be that the NH_3 contribution to nitrate should be small under "rich NH_3" and large under "poor NH_3" environment. Thus, the influence of NH_3 on nitrate formation would enhance with the decreasing of ambient NH_3 mass concentration.

1. Introduction

Ammonia (NH_3) is an important pollution species which principal neutralizing agent for the acid aerosols, SO_4^{2-} and NO_3^- formed from the SO_2 and NO_x (Chang, 1989; McMurry et al.; 1983). In addition, NH_3 also influences the rate of particle nucleation (Ball et al.; 1999; Kulmala et al.; 2002) and enhances secondary organic aerosols (SOA) yields (Babar et al.; 2017). The widespread haze events have frequently occurred in most regions of eastern China in recent years, and several studies have reported that the secondary inorganic salts, including sulfate, nitrate, and ammonium, were the majorities of the total aerosols in the urban and rural regions (Tao et al.; 2014; Wang et al.; 2016; Zhang et al.; 2012; Lai et al.; 2016; Zhang et al.; 2018). Therefore, besides the heavy emissions of SO_2 and NO_2, NH_3 emissions from the agriculture activities are also non-negligible.

China is one of the largest agriculture country in the world. Even though a decrease appeared from 2006 to 2012, the annual emission budget of NH_3 which reached 9.7-12 Tg (Kang et al.; 2016; Xu et al.; 2016; Zhou et al.; 2015) was still huge and leads to high NH_3 ambient concentration. This massive NH_3 significantly affects the regional air quality and horizontal visibility. Firstly, the major $PM_{2.5}$ components, $(NH_4)_2SO_4$, $(NH_4)_3H(SO_4)_2$, NH_4HSO_4, and NH_4NO_3 were partially or fully yielded from neutralizing H_2SO_4 and HNO_3 by the NH_3 reacts (Tanner et al.; 1981; Brost et al.; 1988; Quan et al.; 2014; Zhao et al.; 2013; Zhang et al.; 2014). Studies also showed that NH_3 improves the H_2SO_4 nucleation by 1-10 times (Benson et al.; 2011), and provides sufficient new particle to alter the number and size distributions. Thus, the NH_3 and its secondary product NH_4^+ play an important role in the formation of air pollution and haze days. Some research showed that about 80% of total anthropogenic NH_3 emissions derived from the agriculture sources, and the livestock manure provided more contributions than that of the synthetic fertilizer (Kang et al. 2016; Zhou et al.; 2016). The Chinese government has taken several control strategies to reduce the particle pollutions and their precursors, such as the catalytic reduction systems in the power sector (Xia et al.; 2016), measures to change coal to gas for residents' life and heating (Ren et al.; 2014), etc. Related observations have shown that the mass burden of SO_2 and NO_x have distinctly decreased in recent year (De Foy et al.; 2016; Wang et al.; 2015; Zheng et al.; 2018). However, there was no specific measures for agriculture NH_3 emission control have been implemented until now and the total agriculture NH_3 emission budget was not obviously changed from 2010 to 2017 (Zheng et al.; 2018).

In addition, an accurate information of agriculture NH_3 emission is also important for estimating the NH_3 mass burden and its environmental effect. There were several studies focusing on NH_3 emissions from

agricultural activities in China or East Asia. REAS (Regional Emission inventory in Asia) version 2 established an anthropogenic emission inventory which includes the source of agricultural NH_3 (fertilizer application and livestock) (Kurokawa et al.; 2013). This inventory targeting years from 2000 to 2008 has 0.25×0.25 degree spatial resolution with monthly variation. MASAGE_NH_3 (Magnitude and Seasonality of Agricultural Emissions model for NH_3) developed a bottom-up NH_3 emission inventories by using the adjoint of the GEOS-Chem chemical transport model (Paulot et al.; 2014). The network data for NH_4^+ wet deposition fluxes from 2005-2008 were inversed to optimize the NH_3 emission in China in this inventory. Fu et al. (2015) used CMAQ model coupled to an agro-ecosystem to estimate the NH_3 emissions with high spatial and temporal resolution in 2011, which could obtain hourly emission features by online model calculation. These NH_3 emission inventory provided very useful datasets for understanding the distribution features of NH_3 mass burden in China. However, with the migration of population, economic growth, and increasing of agricultural products consumption, the spatial distribution and strength of agriculture NH_3 emission was significantly changed in China during last decade (Xu et al.; 2017), so that a reliable emission information based on recent year is also necessary for estimating the NH_3 mass burden.

Previous studies have investigated the influence of NH_3 emission to aerosol loading in several typical areas of China. Wu et al. (2008) conducted sensitivity studies to assess the impact of the livestock NH_3 emissions on $PM_{2.5}$ mass concentration in North China by using MM5/CMAQ modeling system. The results showed that the livestock NH_3 provided >20% contributions to nitrate and ammonium, but provided quite small contribution to sulfate. Wang et al. (2011) used the response surface modeling technique to estimate the NH_3 emission contribution in the East China, and found that the total NH_3 emission contributed 8-11% to $PM_{2.5}$ concentration, and the nonlinear effects were significant while the transition between NH_3 rich and poor conditions. Fu et al. (2017) and Zhao et al. (2017) also investigated the impact of NH_3 emission on $PM_{2.5}$ in East China and Hai River Basin. However, the related research was still less and mainly focused on the local regions, and most of them generally used the brute-force sensitivity method to estimate the NH_3 impact based on chemistry model, which reflect the particle concentration change with emission reduction (Koo et al.; 2009).

A comprehensive high-resolution NH_3 emission inventory PKU-NH_3 based on the year 2015 is applied in this study to capture the agriculture NH_3 mass concentration in China, and the contribution to $PM_{2.5}$ particle was estimated by an air quality modeling system RAMS-CMAQ coupled with the online source tagged module ISAM. Compared with previous studies, this high-resolution agriculture NH_3 emission

inventory is more accurate and reflects the latest spatial and temporal distribution features (Liu et al.; 2019). The major trace gases and aerosol species in 2015 were simulated by the modeling system and evaluated by several observation data. The contribution to the pollutant concentrations can be tagged and quantified by RAMS-CMAQ-ISAM under current scenario (Wang et al.; 2009). Then, several brute-force sensitivity tests were conducted to estimate the effect of reducing agriculture NH_3 emission on the $PM_{2.5}$ mass burden as well. The results from the source apportionment simulation and brute-force sensitivity tests in January, April, July, and October were present, and the detail features over seven major populated areas (as shown in Figure 1) of China were mainly discussed.

2. Methodology

The emission inventory was described as follow. Firstly, the NH_3 emission data in China was provided by the PKU-NH_3 emission inventory (Kang et al.; 2016; Zhang et al.; 2018). This inventory was developed on the basis of previous studies (Huang et al.; 2012) and improved the horizontal resolution and accuracy. It compiled on 1km×1km horizontal resolution with monthly based statistic data in 2015. One of the most uncertainty parameter the emission factors applied in this inventory was enhanced by considering as many native experiment results as possible with ambient temperature, soil acidity, and other factors change. In addition, this inventory not only includes the fertilizer and husbandry emission from agriculture activities, but also collects the emission data of farmland ecosystems, livestock waste, biomass burning (forest and grassland fires, crop residue burning, and fuel wood combustion), and other sources (excrement waste from rural populations, the chemical industry, waste disposal, NH_3 escape from thermal power plants, and traffic sources). Secondly, the anthropogenic emission of primary aerosols and the precursors were obtained from the MIX Asian emission inventory (base year 2012) prepared by the Model Inter-Comparison Study for Asia (MICS-ASIA III) (Lu et al.; 2011; Lei et al.; 2011). The anthropogenic emission sources of SO_2, NO_x, volatile organic compounds (VOCs), black carbon (BC), organic carbon (OC), primary $PM_{2.5}$, and PM_{10} were obtained from the monthly-based MIX inventory with 0.25°× 0.25° spatial resolution. The REAS (Regional Emission Inventory in Asia; Version 2; Kurokawa et al.; 2013) and GFED (Global Fire Emissions Database; Version 3; van der Werf et al.; 2010) were used to provide the VOCs, nitrogen oxides from flight exhaust, lighting, paint, wildfires, savanna burning, and slash-and-burn agriculture.

The modeling system RAMS-CMAQ was applied to simulate the transformation and transport of pollutants in atmosphere. The regional air quality model CMAQ (version 5.0.2) released by US

Environmental Protection Agency (Eder et al.; 2009; Mathur et al.; 2008) was the major component of the RAMS-CMAQ modeling system. In this model, The CB05 (version CB05tucl) chemical mechanism (Whitten, 2010) was used to treat the gas-phase chemical mechanism. The simulation of O_3 in urban plumes, which could impacts the NO_x chemical transformation and fine particle mass predictions, was updated in this version for obtaining more reasonable results. The sixth-generation model CMAQ aerosol model (AERO6) which added 9 new $PM_{2.5}$ species and updated the secondary organic aerosol (SOA) yield parametrization and primary organic aerosol (POA) aging processes was used to simulate the formation and dynamic processes of aerosols. ISORROPIA model (version 2.1) (Fountoukis and Nenes, 2007) was used to describe the thermodynamic equilibrium of gas-particle transformation. The highly versatile numerical model RAMS which can well capture the boundary layer and the underlying surface was applied to provide the meteorological fields for CMAQ (Cotton et al.; 2003). The European Centre for Medium-Range Weather Forecasts reanalysis datasets (1°×1° spatial resolution) were used to supply the background fields and sea surface temperatures. The model domain (Figure 1) is 6654 km × 5440 km with 64 km^2 fixed grid cells, and uses a rotated polar stereographic map projection covered the whole mainland of China and its surrounding regions. The model has 15 vertical layers and half of them are located in the lowest 2 km to provide more precise simulation of the atmospheric boundary layer.

The ISAM is a flexible and efficient on-line source apportionment implementation which was used to track multiple pollutants emitted from different geographic regions and source types. Compared with its previous version TSSA (Tagged Species Source Apportionment), the processes of tracking tagged tracer transport and precursor reaction were optimized for balancing the computational requirements and reliable representation of the physical and chemical evolution. In order to reduce the nonlinear effect during phase transformation and relative chemical interactions, a standalone subroutine "wrapper" approach was applied in ISAM to apportion the secondary PM species and their precursor gases during the thermodynamic equilibrium simulation; a hybrid approach which employing the LU decomposition triangular matrices (Yang et al.; 1997) was developed for describing the gas-phase chemical interactions as well. In this study, ISAM was coupled into RAMS-CMAQ and set to trace the transport and chemical reactions of the NH_3 from fertilizer and husbandry emission sectors for quantitatively estimating the contribution of agriculture NH_3 emission to the $PM_{2.5}$ mass concentration in China.

3. Model evaluation

In order to evaluation the model performances, several observation data are used to compared with the simulation results. The meteorological factors are important to capture the formation processes and transport of secondary aerosols. Thus, in this paper, the observed meteorological data from surface stations of the Chinese National Meteorological Center are collected to evaluate the performance of the model. The detail information is described in Appendix A. Furthermore, the observed SO_2, NO_2, and $PM_{2.5}$ released from the Ministry of Environmental Protection of China were applied to evaluate the modeled mass concentration of these pollutants. The hourly observation data in January, April, July and October at 6 stations that located in Beijing, Jinan, Shijiazhuang, Nanjing, Guangzhou and Zhengzhou were collected in this study. The scatter plots of comparison are shown in Figure 2, and the statistical parameters between the observations and simulations are listed in Table 1-3. It can be seen that most of the scatter points broadly gather around the 1:1 solid line. Most of the correlation coefficients in Table 1-3 are higher than 0.5, which indicates that the model can capture the regional variation features of measurements. The standard deviations between the observation and simulation were similar in most cases as well. The simulation results performed better in winter than that in summer because the diffusion condition was strong and the mass concentration changed noticeably during summer time. The modeled $PM_{2.5}$ generally performed well due to relatively high correlation coefficients. The obvious deviation of the modeled mean, which was higher than that of the observation, was between the observed and modeled SO_2. The emission of SO_2 reduced rapidly because of the control measures from 2013 in China. However, the emission inventory may not reflect this feature and slightly overestimated the mass burden.

The horizontal distributions of modeled monthly NH_3 mass concentration in January, April, July, and October in 2015 are shown in Figure 3. Pan et al. (2018) provided the distributions of satellite NH_3 total column distribution and the surface NH_3 concentrations at several observation sites in their Figure 1. As shown from their results, the highest mass burden mainly concentrated in North China Plain (NCP), Central China (CNC), Yangtz River Delta (YRD), and Sichan Basin (SCB). The simulation results in this study broadly reflected these distribution features. The values of NH_3 concentrations in these regions could reach 10-25 $\mu g\ m^3$ in Pan et al. (2018), which also coincided well with the simulation results. However, some obvious deviation appeared in the areas of east part of Gansu province. The modeled NH_3 in these regions by this study was slightly higher than those of the observations in Pan et al. (2018). Zhang et al. (2018) also showed the NH_3 mass concentration in four seasons over China from simulation (horizontal distribution) and ground-based measurements (point values) in their Figure 9. Besides the regions maintained in Pan et

al. (2018), the high mass burden of NH_3 also appeared in the Northeast China (NEC) as shown by both simulation and observation in Zhang et al. (2018). Generally, this distribution feature should be reasonable because the Three River Plain located in NEC is an important agriculture base of China, and the NH_3 emission in this region can be strong during spring and summer. The simulation results in this study also followed the seasonal variation feature of NH_3 mass burden as shown in Zhang et al. (2018), which was higher in summer and lower in winter, and the magnitude was also close with each other. Thus, it can be seen that the modeled NH_3 concentration by RAMS-CMAQ was reliable and can be applied for the analysis in this study.

4. Results and discussions

The horizontal distributions of modeled monthly $PM_{2.5}$ mass concentration in January, April, July, and October in 2015 was shown in Figure 4. The surface wind field was also shown in Figure 4. Over the east part of China, the heavy $PM_{2.5}$ pollution happened in January and the relatively better air quality appeared in July. The large $PM_{2.5}$ mass burden exceeded 200 μg m^3 in January mainly concentrated in the NCP, the Yangtze River Valley of CNC, and SCB, which broadly coincided with the regions covered by high mass burden of NH_3 as shown in Figure 3. It can be seen that the wind speed in the regions mentioned above was relatively weak, implying that the diffusion condition was not good, and more aerosol can be trapped in these region. In addition, the $PM_{2.5}$ mass burden (50-150 μg m^{-3}) was obviously lower than other months in July. Since the NH_3 emission mainly concerns with the secondary inorganic aerosols (SNA): sulfate, nitrate, and ammonium formation, the analysis hereafter will mainly focus on the SNA. Figure 5 present the modeled monthly SNA mass concentration in January, April, July, and October in 2015. The mass loading of SNA generally provided 40-60% to the total $PM_{2.5}$ in the east part of China, which was comparable with previous studies (Cao et al.; 2017; Chen et al.; 2016; Lai et al.; 2016; Wang et al.; 2016). The distribution pattern and seasonal variation of SNA also followed the features of $PM_{2.5}$, and the high mass concentration of SNA could exceed 100 μg m^{-3} in January.

Then, the contributions of NH_3 from the multiple agriculture emission (includes fertilizer, husbandry, farmland ecosystems, livestock waste, crop residue burning, and excrement waste from rural populations) to aerosols were calculated using RAMS-CMAQ-ISAM; the monthly average contribution percentage of total agriculture activities (Tagr) in January, April, July, and October are shown in Figure 6. Generally, the Tagr NH_3 provided 30-50% contribution in January and October, and 20-40% contribution in April and

July to the SNA over the most part of east China. The relatively lower value mainly appeared in April.

The regional average percent of Tagr contribution to sulfate, nitrate, ammonium, SNA, and $PM_{2.5}$ are shown in Table 4. As shown in this table, the annually average Tagr NH_3 provided major contribution which reached about 90% to ammonium and relatively small contribution which was 5-10% to nitrate mass burden. However, the contribution to sulfate was tiny and the main reason should be that there are various ways of sulfate formation from SO_2 besides neutralized by NH_3, such as oxidized by H_2O_2, O_3, or peroxyaceticn acid. The seasonal variation of ammonium was obvious: it could higher than 99% in January but lower than 70% in July. Most of the difference as shown in Table 4 could exceeded 10% because the NH_3 emitted from other sources (anthropogenic and natural sources) was significant in these regions during summer time. The annually average Tagr NH_3 provided 20-40% contribution to the SNA mass concentration, and the contributions in January were larger than that in July as well. The seasonal variation and spatial features of Tagr NH_3 contribution to $PM_{2.5}$ mass concentration were similar with the features of SNA, and generally provided approximate 14-22% contribution to the total $PM_{2.5}$ mass concentration in these places. On the other hand, it can be seen that the annual contribution in China were higher than those of the contribution in the regions mentioned above. This feature indicated that the Tagr NH_3 provided more contribution than other sources over the regions with weaker anthropogenic activities.

In addition, the brute-force method (zero-out sensitivity test) which can capture the effect of emissions change on aerosol mass burden was applied to investigate the impact of the removal of Tagr NH_3 emission. Unlike the on-line source apportionment, the brute-force method mainly reflects the disparity of chemical balance caused by the emissions change, which could significantly alter the secondary pollutant formation. Several sensitivity tests were conducted and the results are shown in Figure 7 and Table 5. Figure 7 presents the mass burden variation of SNA associated with the Tagr NH_3 removal. From Figure 7, it can be seen that the reduction pattern and seasonal variation of the aerosol were broadly followed those of their mass burden. The significant reduction of SNA mainly appeared in the high concentration regions, and generally exceeded 25 $\mu g\ m^{-3}$. Table 5 shows the percentage of the variation of sulfate, nitrate, ammonium, SNA, and $PM_{2.5}$. Compared with Table 4, it can be found that the variation percent of SNA and $PM_{2.5}$ which reached 30-60% and 24-42%, respectively, were about two times higher than those of the contribution percent, and this significant distinction was mainly caused by the variation of nitrate: the contribution of Tagr NH_3 to nitrate was generally below 10% as shown in Table 4, but the reduction of nitrate associated with removing Tagr NH_3 emission could exceed 90% as shown in Table 5. This difference between the results of ISAM

and brute-force was expected as a result of high nonlinearity in the NO_x chemistry. The nitrate formation could become more sensitive when the "rich NH_3" environment shifts to "poor NH_3" environment, which means the decrease of nitrate mass burden would accelerate with the NH_3 emission reduction. Therefore, it can be deduced that the contribution of NH_3 to nitrate should be significantly lower under "rich NH_3" environment than that under "poor NH_3" environment. Similar phenomenon was also reported by some previous study (Wang et al.; 2011; Xu et al.; 2016). To prove this point, more brute-force sensitivity tests were conducted. The variation of sulfate, nitrate, ammonium, and SNA mass burden associated with the reduction of NH_3 emission (80%, 50%, 40%, 30%, 20%, and 10% Tagr NH_3 emission, respectively) was shown in Figure 8. It can be seen that the decline of nitrate mass concentration was more rapid than that of ammonium, and the trend became slightly faster with the reduction of NH_3 emission (signifying from "rich NH_3" to "poor NH_3") in the most regions. The acceleration of nitrate mass burden decline was more significant in the regions with strong NH_3 emission. Furthermore, this acceleration stopped while 20% NH_3 emission remained as shown in Figure 8.

5. Conclusions

The emission budget of agriculture NH_3 was huge and played an important role on the regional particle pollution in China. As a precursor of the secondary aerosol, reasonably estimate the nonlinear processes of secondary aerosol formation should be the key point for capturing the contribution of NH_3 to particle pollution. In this study, the air quality modeling system RAMS-CMAQ was applied to simulate spatial-temporal distribution of trace gas and aerosols in 2015. In addition, the PKU-NH_3 emission inventory which compiled on 1km×1km horizontal resolution with monthly based data was applied to accurately capture the agriculture NH_3 emission features in China. Then, the source apportionment module ISAM was coupled into this modeling system to quantitatively estimate the contribution of agriculture NH_3 to $PM_{2.5}$ mass burden. The brute-force sensitivity tests were also conducted for discussing the impact of the agriculture NH_3 emission reduction. The meteorological factors and mass concentration of NH_3, SO_2, NO_2, and $PM_{2.5}$ from simulation were evaluated and showed well agreement with the observation data. Some interesting results were explored and summarized as follow:

(1) The high mass burden of NH_3 could exceeded 10 μg m^{-3}, and mainly appeared in the NCP, CNC, YRD, and SCB. These regions were highly coincidence with the regions that heavy particle pollution covered in China. Therefore, it can be deduced that the influence of agriculture NH_3 on the $PM_{2.5}$ mass

concentration should be significant.

(2) The results from ISAM simulation shows that the Tagr NH_3 provided 17-23% and 15-22% contribution to the $PM_{2.5}$ in January and July, respectively, in the most part of east China, and the largest annual average contribution appeared in CNC (17.5%). Specific to the SNA components, the annually and regional average contribution of Tagr NH_3 to ammonium, nitrate, sulfate was 87.6%, 10.1%, and 2.2% in China. The agriculture NH_3 emission provided major contribution to the ammonium formation, but tiny contribution to the sulfate due to the various other ways of sulfate formation.

(3) The brute-force sensitive test could reflect the effect of changing Tagr NH_3 emission on $PM_{2.5}$ mass burden. The results indicated that the reduction percent of $PM_{2.5}$ mass burden due to removal Tagr NH_3 emission could reach 24-42% in the most part of east China, which was approximately two times higher than the contribution. The reduction percent of nitrate that reached exceed 90% was the main reason caused this significant different. In addition, the further analysis proved that the ambient NH_3 mass burden could obviously affects its contribution to the SNA formation: the NH_3 contribution to nitrate should be lower under "rich NH_3" and higher under "poor NH_3". Therefore, the influence of NH_3 would enhance with the decreasing of ambient NH_3 mass concentration.

It is suggested that the NH_3 influence on the $PM_{2.5}$ mass burden are complex because of the nonlinearity of secondary aerosol formation. Significantly deviation exists between the results from ISAM and brute-force method, so that these two kinds of results should be distinguished and applied to explain different issues: the contribution under current scenario and the effect due to emission reduction, respectively. The modeling system is a versatile tool allows us to investigate these valuable information for choosing more efficient strategies of reducing the impact of agriculture NH_3 and improving air quality.

Acknowledgments

This work was supported by the Strategic Priority Research Program of the Chinese Academy of Sciences (XDA19040204), and the National Natural Science Foundation of China (41830109).

Appendix A

The daily average temperature, relative humidity, wind speed and maximum wind direction in January, April, July and October 2015 were compared with the surface shared data from the Chinese National Meteorological Center (http://data.cma.cn/) in 9 stations. The comparison results are shown in Figure A1-A4. These stations are located in the East China where the high NH_3 emission regions. Generally, the modeled temperature was in good agreement with the observed data, and can reflect the large fluctuation and seasonal variation of relative humidity as well, except that some of the extreme high or low values appeared abruptly. As shown in Figure A3, most of the daily average wind speed was lower than 3 m s^{-1} at Zhengzhou, Miyun, Tianjin and Baoding station (all located in the North China Plain), which means the diffusion condition was not good due to the stable weather. Otherwise, the relatively strong wind appeared at Nanjing, Chaoyang, Nanning and Jinan. The modeled wind speed generally reproduced all these features. The direct comparison between observed and modeled wind direction which can be easily influenced by the surrounding surface features is difficult. Nevertheless, the prevailing wind direction in different seasons can be captured by the simulation results for all stations.

In addition, Figure A5 present the regional average NH_3 emission flux (g/s/grid) of different sectors, including fertilizer, Husbandry, Biomass burning, Farmland ecosystems, Waste disposal, and other sectors, over each regions in January, April, July and October. Furthermore, the percent (%) of each NH_3 emission sector was shown in Figure A6. All the information was obtained from the PKU-NH_3 emission inventory directly. It can be seen that the emission flux was higher in summer and lower in winter. The strongest emission flux mainly appeared in BTH, SDP and CNC. The distribution pattern of NH_3 mass concentration

These features generally followed the distribution pattern of NH_3 mass concentration as shown in Figure 3. On the other hand, the major proportion was provided by husbandry and fertilizer, and relatively higher in spring and summer.

Reference

Babar, Z. B.; Park, J.; Lim, H. Influence of NH_3 on secondary organic aerosols from the ozonolysis and photooxidation of a -pinene in a flow reactor. *Atmos. Environ.* 2017, 164, 71-84, DOI: 10.1016/j.atmosenv.2017.05.034

Ball, S. M.; Hanson, D. R.; Eisele, F. L.; McMurry, P. H. Laboratory studies of particle nucleation: Initial results for H_2SO_4, H_2O, and NH_3 vapors. *J. Geophys. Res.* 1999, 104, 23709-23718, DOI: 10.1029/1999JD900411

Benson, D. R.; Yu, J. H.; Markovich, A.; Lee, S. H. Ternary homogeneous nucleation of H_2SO_4, NH_3, and H_2O under conditions relevant to the lower troposphere. *Atmos. Chem. Phys.* 2011, 11, 4755-4766, DOI: 10.5194/acp-11-4755-2011

Brost, R. A.; Delany, A. C.; Huebert, B. J. Numerical modeling of concentrations and fluxes of HNO_3, NH_3, and NH_4NO_3 near the ground. *J. Geophys. Res.* 1988, 93, 7137-7152, DOI: 10.1029/JD093iD06p07137

Cao, Z.; Zhou, X.; Ma, Y.; Wang, L.; Wu, R.; Chen, B.; Wang, W. The concentrations, formations, relationships and modeling of sulfate, nitrate and ammonium (SNA) aerosols over China. *Aerosol Air Qual. Res.* 2017, 17, 84-97, DOI: 10.4209/aaqr.2016.01.0020

Chen, Y.; Schleicher, N.; Cen, K.; Liu, X.; Yu, Y.; Zibat, V.; Dietze, V.; Fricker, M.; Kaminski, U.; Chen, Y.; Chai, F.; Norra, S. Evaluation of impact factors on $PM_{2.5}$ based on long-term chemical components analyses in the megacity Beijing, China. *Chemosphere* 2016, 155, 234-242, DOI: 10.1016/j.chemosphere.2016.04.052

Chang, J. The role of H_2O and NH_3 on the formation of NH_4NO_3 aerosol particles and De-NOx under the corona discharge treatment of combustion flue gases. *J. Aerosol Sci.* 1989, 20, 1087-1090, DOI: 10.1016/0021-8502(89)90768-4

Cotton, W.; Pielke, R.; Walko, G.; Liston, G.; Tremback, C.; Jiang, H.; McAnelly, R.; Harrington, J.; Nicholls, M.; Carrio, G.; McFadden, J. RAMS 2001: current status and future directions, Meteorol. *Atmos. Phys.* 2003, 82, 5-29, DOI:

DeFoy, B.; Lu, Z.; and Streets, D. G. Satellite NO_2 retrievals suggest China has exceeded its NO_x reduction goals from the twelfth five-year plan. *Sci. Rep.* 2016, 6, 35912, DOI: 10.1007/s00703-001-0584-9

Eder, B.; Yu S. A performance evaluation of the 2004 release of Models-3 CMAQ. *Atmos. Environ.* 2006, 40, 4811-4824, DOI: 10.1016/j.atmosenv.2005.08.045

Fountoukis, C.; Nenes, A. ISORROPIA II: a computationally efficient thermodynamic equilibrium model for K^+-Ca^{2+}-Mg^{2+}-NH_4^+-Na^+-SO_4^{2-}-NO_3^- -Cl^--H_2O aerosols. *Atmos. Chem. Phys.* 2007, 7, 4639-4659, DOI: 10.5194/acp-7-4639-2007

Fu, X.; Wang, S.; Xing, J.; Zhang, X.; Wang, T.; Hao, J. Increasing Ammonia Concentrations Reduce the Effectiveness of Particle Pollution Control Achieved via SO_2 and NO_x Emissions Reduction in East China. *Environ. Sci. Technol.* 2017, 4, 221-227, DOI: 10.1021/acs.estlett.7b00143

Huang, X.; Song, Y.; Li, J.; Huo, Q.; Cai, X.; Zhu, T.; Hu, M.; Zhang, H. A high-resolution ammonia emission inventory in China. *Global Biogeochem. Cy.* 2012, 26, 1030-1044, DOI: 10.1029/2011GB004161

Kang, Y.; Liu, M.; Song, Y.; Huang, X.; Yao, H.; Cai, X.; Zhang, H.; Kang, L.; Liu, X.; Yan, X.; He, H.; Zhang, Q.; Shao, M.; Zhu, T. High-resolution ammonia emissions inventories in China from 1980 to 2012. *Atmos. Chem. Phys.* 2016, 16, 2043-2058, DOI: 10.5194/acpd-15-26959-2015

Koo, B.; Wilson, G.; Morris, R.; Dunker, A.; Yarwood, G. Comparison of Source Apportionment and Sensitivity Analysis in a Particulate Matter Air Quality Model. *Environ. Sci. Technol.* 2009, 43, 6669-6675

Kurokawa, J.; Ohara, T.; Morikawa, T.; Hanayama, S.; Maenhout, G.; Fukui, T.; Kawashima, K.; Akimoto, H. Emissions of air pollutants and greenhouse gases over Asian regions during 2000-2008: Regional Emission inventory in ASia (REAS) version 2. *Atmos. Chem. Phys.* 2013, 13, 11019-11058, DOI: 10.5194/acp-13-11019-2013

Kulmala, M.; Korhonen, P.; Napari, I.; Karlsson, A.; Berresheim, H.; O'Dowd, C. D. Aerosol formation during PARFORCE: Ternary nucleation of H_2SO_4, NH_3, and H_2O. *J. Geophys. Res.* 2002, 107, DOI: 10.1029/2001JD000900.

Lai, S.; Zhao, Y.; Ding, A.; Zhang, Y.; Song, T.; Zheng, J.; Ho, K. F.; Lee, S.; Zhong, L. Characterization of $PM_{2.5}$ and the major chemical components during a 1-year campaign in rural Guangzhou. *Southern China, Atmos. Res.* 2016, 167,

208-215, DOI: 10.1016/j.atmosres.2015.08.007

Lei, Y.; Zhang, Q.; He, K.; Streets, D. Primary anthropogenic aerosol emission trends for China, 1990-2005. *Atmos. Chem. Phys.* 2011, 11, 931-954, DOI: 10.5194/acp-11-931-2011

Liu, M.; Huang, X.; Song, Y.; Tang, J.; Cao, J.; Zhang, X.; Zhang, Q.; Wang, S.; Xu, T.; Kang, L.; Cai, X.; Zhang, H.; Yang, F.; Wang, H.; Yu, J.; Lau, A.; He, L.; Huang, X.; Duan, L.; Ding, A.; Xue, L.; Gao, J.; Liu, B.; Zhu, T. Ammonia emission control in China would mitigate haze pollution and nitrogen deposition, but worsen acid rain. *PNAS*, 2019, 116, 7760-7765, DOI: 10.1073/pnas.1814880116

Lu, Z.; Zhang, Q.; Streets, D. G. Sulfur dioxide and primary carbonaceous aerosol emissions in China and India, 1996-2010. *Atmos. Chem. Phys.* 2011, 11, 9839-9864, DOI:

Mathur, R.; Yu, S.; Kang, D.; Schere, K. Assessment of the winter-time performance of developmental particulate matter forecasts with the Eta-CMAQ modeling system. *J. Geophys. Res.* 2008, 113, DOI: 10.1029/2007JD008580,

McMurry, P. H.; Takano, H.; Anderson, G. R. Study of the ammonia (gas)-sulfuric acid (aerosol) reaction rate. *Environ. Sci. Technol.* 1983, 17, 347-352, DOI: 10.1021/es00112a008

Paulot, F.; Jacob, D. J.; Pinder, R. W.; Bash, J. O.; Travis, K.; Henze, D. K. Ammonia emissions in the United States, European Union, and China derived by high-resolution inversion of ammonium wet deposition data: Interpretation with a new agricultural emissions inventory (MASAGE_NH3). *J. Geophys. Res.* 2014, 119, 4343-4364, DOI: 10.1002/2013JD021130

Pen, Y.; Tian, S.; Zhao, Y.; Zhang, L.; Zhu, X.; Gao, J.; Huang, W.; Zhou, Y.; Song, Y.; Zhang, Q.; Wang, Y. Identifying ammonia hotspots in China using a national observation network. Environ. Sci. Technol. 2008, doi: 10.1021/acs.est.7b05235, DOI: 10.1021/acs.est.7b05235

Quan, J.; Tie, X.; Zhang, Q.; Liu, Q.; Li, X.; Gao, Y.; Zhao, D. Characteristics of heavy aerosol pollution during the 2012–2013 winter in Beijing, China. *Atmos. Environ.* 2014, 88, 83-89, DOI: 10.1016/j.atmosenv.2014.01.058

Ren, H.; Zhang, L.; Hong, X. Politic recommendations on strengthening reduction of air pollutant emissions in China. *Environ. Sustain. Dev.* 2014, 39, 4-13, (in Chinese)

Tao, M.; Chen, L.; Xiong, X.; Zhang, M.; Ma, P.; Tao, J.; Wang, Z. Formation process of the widespread extreme haze pollution over northern China in January 2013: Implications for regional air quality and climate. *Atmos. Environ.* 2014, 98, 417-425, DOI: 10.1016/j.atmosenv.2014.09.026

Tanner, R. L.; Leaderer, B. P.; Spengler, J. D. Acidity of atmospheric aerosols. *Environ. Sci. Technol.* 1981, 15, 1150–1153, DOI: 10.1021/es00092a003

van der Werf, G.; Randerson, J. Giglio, L.; Collatz, G.; Mu, M.; Kasibhatla, P.; Morton, D.; Defries, R.; Jin, Y.; van Leeuwen, T. Global fire emissions and the contribution of deforestation, savanna, forest, agricultural, and peat fires (1997-2009). *Atmos. Chem. Physics.* 2010, 10, 11707-11735, DOI: 10.5194/acp-10-11707-2010

Wang, G.; Zhang, R.; Gomez, M. E.; Yang, L.; Levy Zamora, M.; Hu, M.; Lin, Y.; Peng, J.; Guo, S.; Meng, J.; Li, J.; Cheng, C.; Hu, T.; Ren, Y.; Wang, Y.; Gao, J.; Cao, J.; An, Z.; Zhou, W.; Li, G.; Wang, J.; Tian, P.; Marrero-Ortiz, W.; Secrest, J.; Du, Z.; Zheng, J.; Shang, D.; Zeng, L.; Shao, M.; Wang, W.; Huang, Y.; Wang, Y.; Zhu, Y.; Li, Y.; Hu, J.; Pan, B.; Cai, L.; Cheng, Y.; Ji, Y.; Zhang, F.; Rosenfeld, D.; Liss, P. S.; Duce, R. A.; Kolb, C. E.; Molina, M. J. Persistent sulfate formation from London Fog to Chinese haze. *Proc. Natl. Acad. Sci.* 2016, 113, 13630-13635, DOI: 10.1073/pnas.1616540113

Wang, H.; Qiao, L.; Lou, S.; Zhou, M.; Ding, A.; Huang, H.; Chen, J.; Wang, Q.; Tao, S.; Chen, C.; Li, L.; Huang, C.; 2016, Chemical composition of $PM_{2.5}$ and meteorological impact among three years in urban Shanghai, China. *J. Clean. Prod.* 2016, 112, 1302-1311, DOI: 10.1016/j.jclepro.2015.04.099

Wang, S.; Zhang, Q.; Martin, R.V.; Philip, S.; Liu, F.; Li, M.; Jiang, X.; He, K. Satellite measurements oversee China's sulfur dioxide emission reductions from coal-fired power plants. *Environ. Res. Lett.* 2015, 10, doi: 10.1088/1748-9326/10/11/114015, DOI:

Wang, S.; Xing, J.; Jang, C.; Zhu, Y.; Fu, J.; Hao, J. Impact Assessment of Ammonia Emissions on Inorganic Aerosols in East China Using Response Surface Modeling Technique. *Environ. Sci. Technol.* 2011, 45, 9293-9300, DOI: 10.1021/es2022347

Wang, Z.; Chien, C.; Tonnesen, G. Development of a tagged species source apportionment algorithm to characterize three-dimensional transport and transformation of precursors and secondary pollutants. *J. Geophys. Res.* 2009, 114, DOI: 10.1029/2008JD010846,

Whitten, G.; Heo, G.; Kimura, Y.; McDonald-Buller, E.; Allen, D.; Carter, W. P. L.; Yarwwod, G. A new condensed toluene mechanism for Carbon Bond: CB05-TU. *Atmos. Environ.* 2010, 44, 5346-5355, DOI: 10.1016/j.atmosenv.2009.12.029

Wu, S.; Hu, J.; Zhang, Y.; Aneja, V. P. Modeling atmospheric transport and fate of ammonia in North Carolina-Part II: Effect of ammonia emissions on fine particulate matter formation. *Atmos. Environ.* 2008, 42, 3437-3451, DOI: 10.1016/j.atmosenv.2007.04.022

Xia, Y.; Zhao, Y.; and Nielsen, C. P. Benefits of China's efforts in gaseous pollutant control indicated by the bottom-up emissions and satellite observations 2000-2014. *Atmos. Environ.* 2016, 136, 43-53, DOI: 10.1016/j.atmosenv.2016.04.013

Xu, P.; Liao, Y. J.; Lin, Y. H.; Zhao, C. X.; Yan, C. H.; Cao, M. N.; Wang, G. S.; Luan, S. J. High-resolution inventory of ammonia emissions from agricultural fertilizer in China from 1978 to 2008. Atmos. Chem. Phys. 2016, 16, 1207-1218, DOI: 10.5194/acpd-15-25299-2015

Yang, Y.; Wilkinson, J.; Russell. A. Fast, Direct Sensitivity Analysis of Multi-Dimensional Photochemical Models. *Environ. Sci. Technol.* 1997, 31, 2859-2868, DOI: 10.1021/es970117w

Zhao, Z.; Bai, Z.; Winiwarter, W.; Kiesewetter, G.; Heyes, C.; Ma, L. Mitigating ammonia emission from agriculture reduces $PM_{2.5}$ pollution in the Hai River Basin in China. *Sci. Total Environ.* 2017, 609, 1152-1160, DOI: 10.1016/j.scitotenv.2017.07.240

Zhao, X. J.; Zhao, P. S.; Xu, J.; Meng, W.; Pu, W. W.; Dong, F.; He, D.; Shi, Q. F. Analysis of a winter regional haze event and Its formation mechanism in the North China Plain. *Atmos. Chem. Phys.* 2013, 13, 5685–5696, DOI: 10.5194/acp-13-5685-2013

Zhang, J. K.; Sun, Y.; Liu, Z. R.; Ji, D. S.; Hu, B.; Liu, Q.; Wang, Y. S. Characterization of submicron aerosols during a month of serious pollution in Beijing, 2013. *Atmos. Chem. Phys.* 2014, 14, 2887–2903, DOI: 10.5194/acp-14-2887-2014.

Zhang, K.; Ma, Y.; Xin, J.; Liu, Z.; Ma, Y.; Gao, D.; Wu, J.; Zhang, W.; Wang, Y.; Shen, P. The aerosol optical properties and $PM_{2.5}$ components over the world's largest industrial zone in Tangshan, North China. *Atmos. Res.* 2018, 201, 226-234, DOI: 10.1016/j.atmosres.2017.10.025

Zhang, L.; Chen, Y.; Zhao, Y.; Henze, D.; Zhu, L.; Song, Y.; Paulot, F.; Liu, X.; Pan, Y.; Lin, Y.; Huang, B. Agricultural ammonia emissions in China: reconciling bottom-up and top-down estimates. *Atmos. Chem. Phys.* 2018, 18, 339-355, DOI: 10.5194/acp-18-339-2018

Pan, Y.; Tian, S.; Zhao, Y.; Zhang, L.; Zhu, X.; Gao, J.; Huang, W.; Zhou, Y.; Song, Y.; Zhang, Q.; Wang, Y. Identifying ammonia hotspots in China using a national observation network. *Environ. Sci. Technol.* 2018, doi: 10.1021/acs.est.7b05235, DOI: 10.1021/acs.est.7b05235

Zhang, X.; Wang, Y.; Niu, Y.; Zhang, X.; Gong, S.; Zhang, Y.; Sun, J. Atmospheric aerosol compositions in China: spatial/temporal variability, chemical signature, regional haze distribution and comparisons with global aerosols. *Atmos. Chem. Phys.* 2012, 12, 779-799, DOI: 10.5194/acp-12-779-2012

Zhou, F.; Ciais, P.; Hayashi, K.; Galloway, J.; Kim, D.; Yang, L.; Li, S.; Liu, B.; Shang, Z.; Gao, S. Re-estimating NH_3 emissions from Chinese cropland by a new nonlinear model. *Environ. Sci. Technol.* 2016, 50, 564-572, DOI: 10.1021/acs.est.5b03156

Zhou, Y.; Cheng, S.; Lang, J.; Chen, D.; Zhao, B.; Liu, C.; Xu, R.; Li, T. A comprehensive ammonia emission inventory with high-resolution and its evaluation in the Beijing–Tianjin–Hebei (BTH) region, China. *Atmos. Environ.* 2015, 106, 305-317, DOI: 10.1016/j.atmosenv.2015.01.069

Xu, P.; Koloutsou-Vakakis, S.; Rood, M.; Luan, S. Projections of NH_3 emissions from manure generated by livestock production in China to 2030 under six mitigation scenarios. *Sci. Total Environ.* 2017, 31, 78-86, DOI: 10.1016/j.scitotenv.2017.06.258

Zheng, B.; Tong, D.; Li, M.; Liu, F.; Hong, C.; Geng, G.; Li, H.; Li, X.; Peng, L.; Qi, J.; Yan, L.; Zhang, Y.; Zhao, H.; Zheng, Y.; He, K.; Zhang, Q. Trends in China's anthropogenic emissions since 2010 as the consequence of clean air actions. *Atmos. Chem. Phys.* 2018, 18, 14095-14111, DOI: 10.5194/acp-18-14095-2018

Kurokawa, J.; Ohara, T.; Morikawa, T.; Hanayama, S.; Janssens-Maenhout, G.; Fukui, T.; Kawashima, K.; Akimoto, H. Emissions of air pollutants and greenhouse gases over Asian regions during 2000-2008: Regional Emission inventory in ASia (REAS) version 2. *Atmos. Chem. Phys.* 2013, 13, 11019-11058, DOI: 10.5194/acp-13-11019-2013

Fu, X.; Wang, S.; Ran, L.; Pleim, J.; Cooter, E.; Bash, J.; Benson, V.; Hao, J. Estimating NH_3 emissions from agricultural fertilizer application in China using the bi-directional CMAQ model coupled to an agro-ecosystem model. *Atmos. Chem. Phys.* 2015, 15, 6637-6649, DOI: 10.5194/acp-15-6637-2015

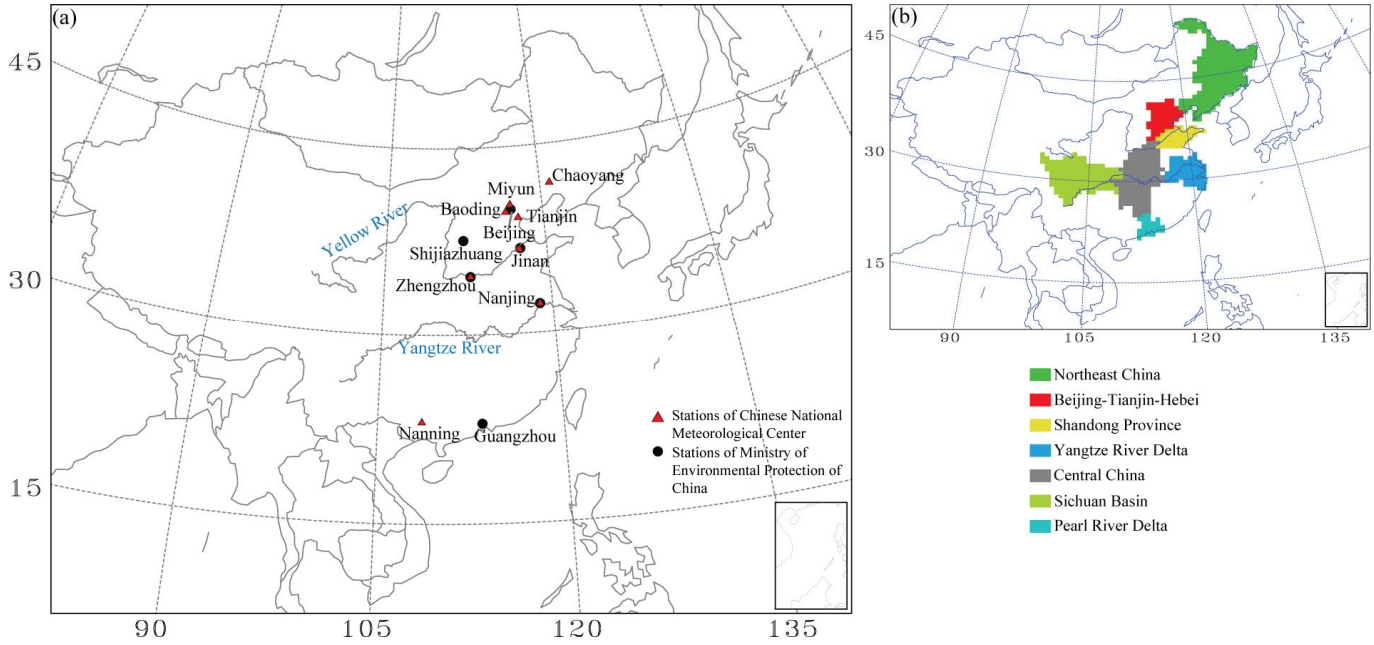

Figure 1. Model domain used in this study and the geographic locations of Beijing-Tianjin-Hebei (BTH), Northeast China (NEC), Yangtze River Delta (YRD), Pearl River Delta (PRD), Sichuan Basin (SCB), Central China (CNC) and Shandong Province (SDP). The location of observation data was also shown in the model domain.

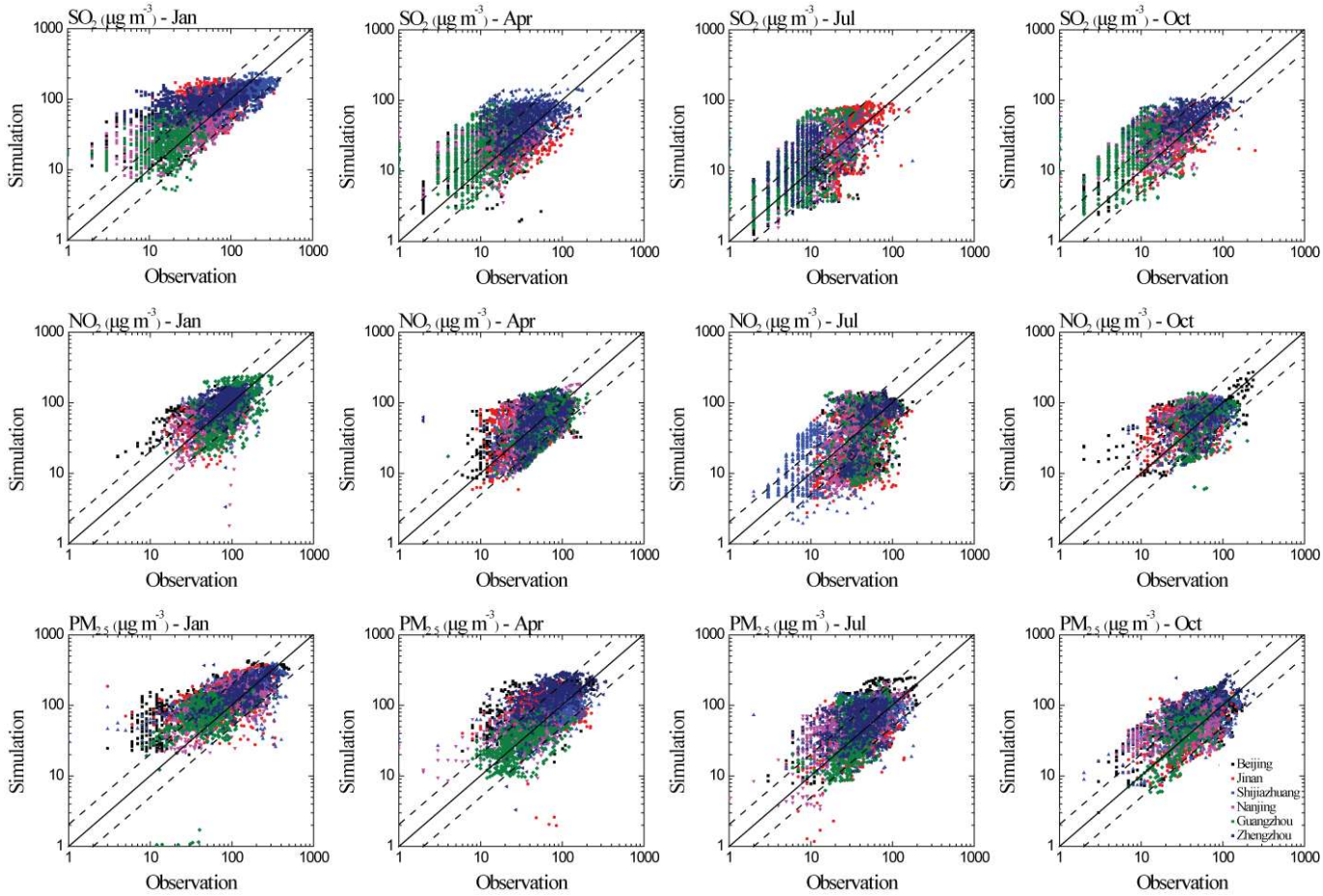

Figure 2. The scatter plots between the modeled and the observed hourly SO_2, NO_2, and $PM_{2.5}$ in January, April, July and October 2015. The solid lines are 1:1 and the dashed lines are 2:1 or 1:2.

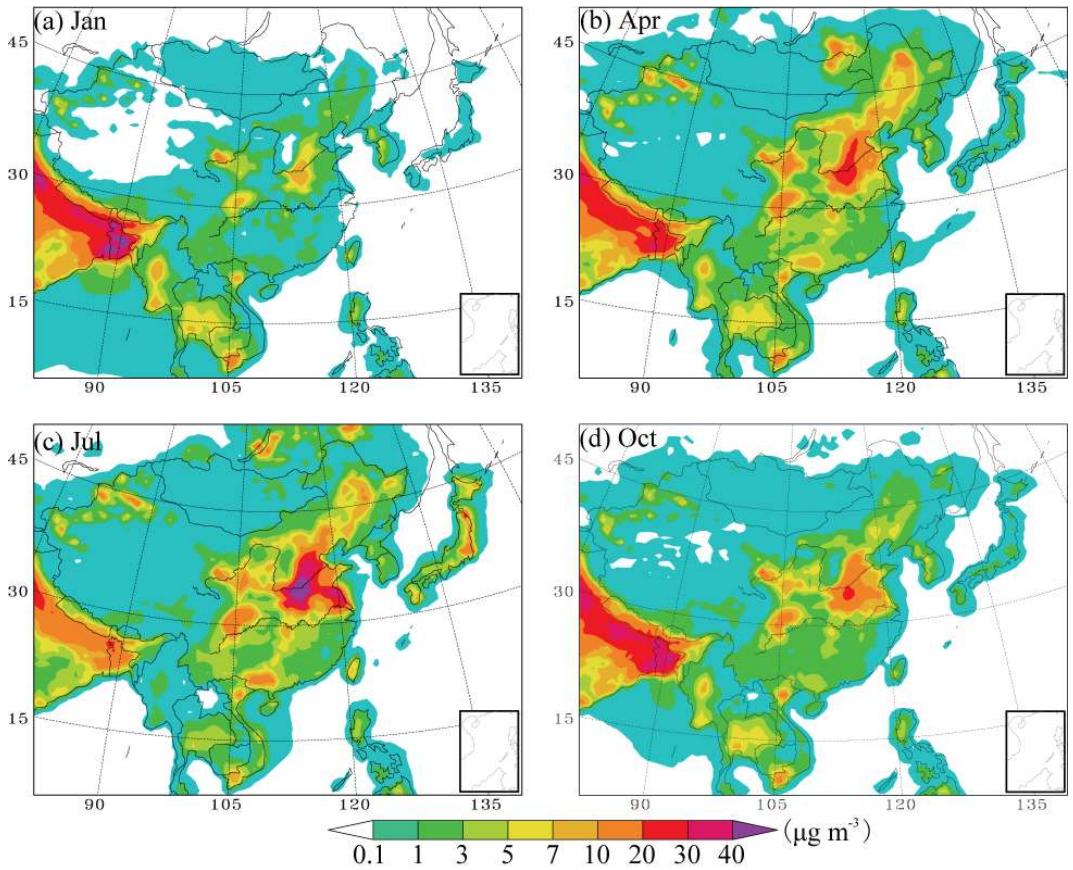

Figure 3. The horizontal distributions of the modeled monthly NH_3 mass concentration in January, April, July, and October in 2015.

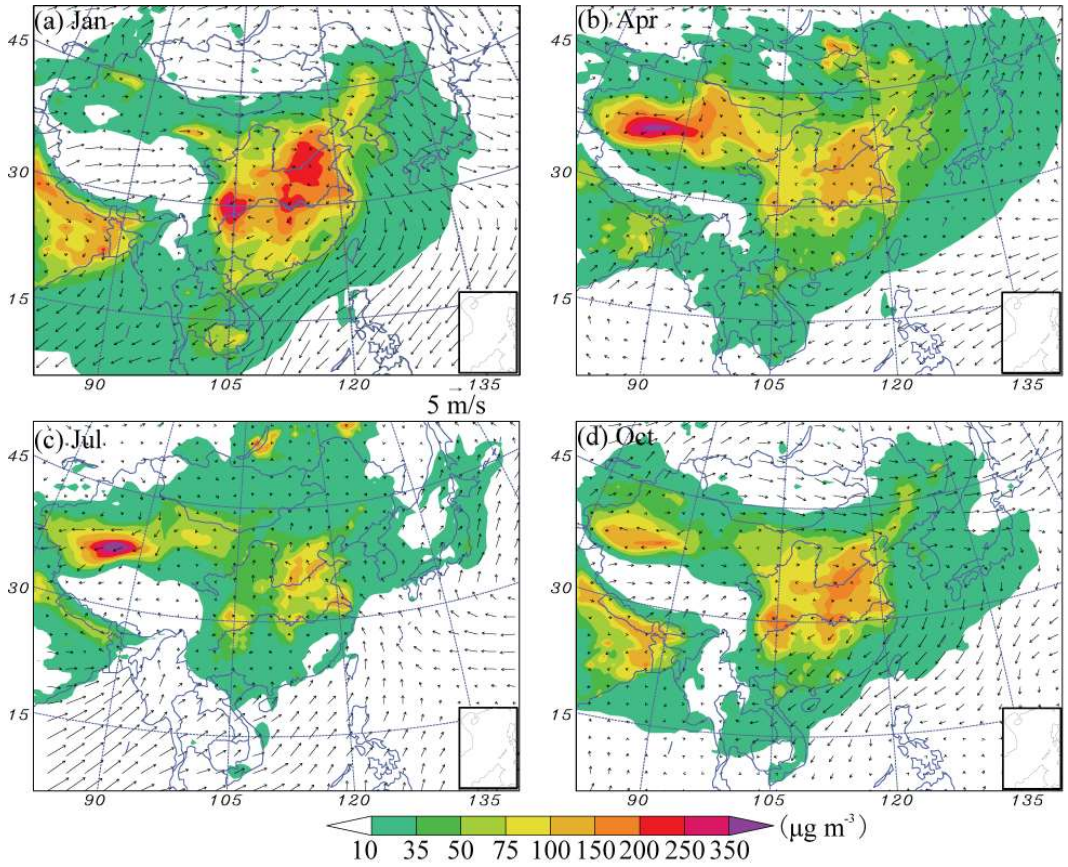

Figure 4. The horizontal distributions of the modeled monthly $PM_{2.5}$ mass concentration in January, April, July, and October in 2015. Also shown are the surface wind field.

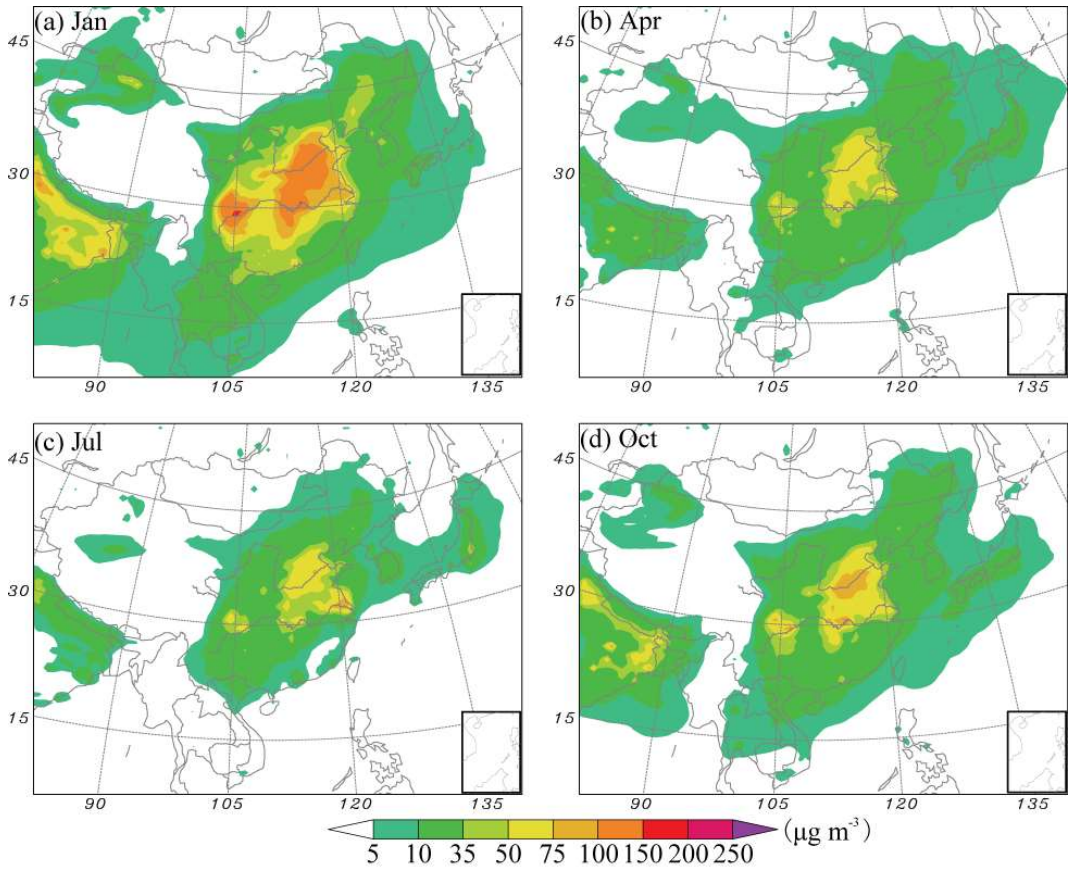

Figure 5. The horizontal distributions of the modeled monthly SNA mass concentration in January, April, July, and October in 2015.

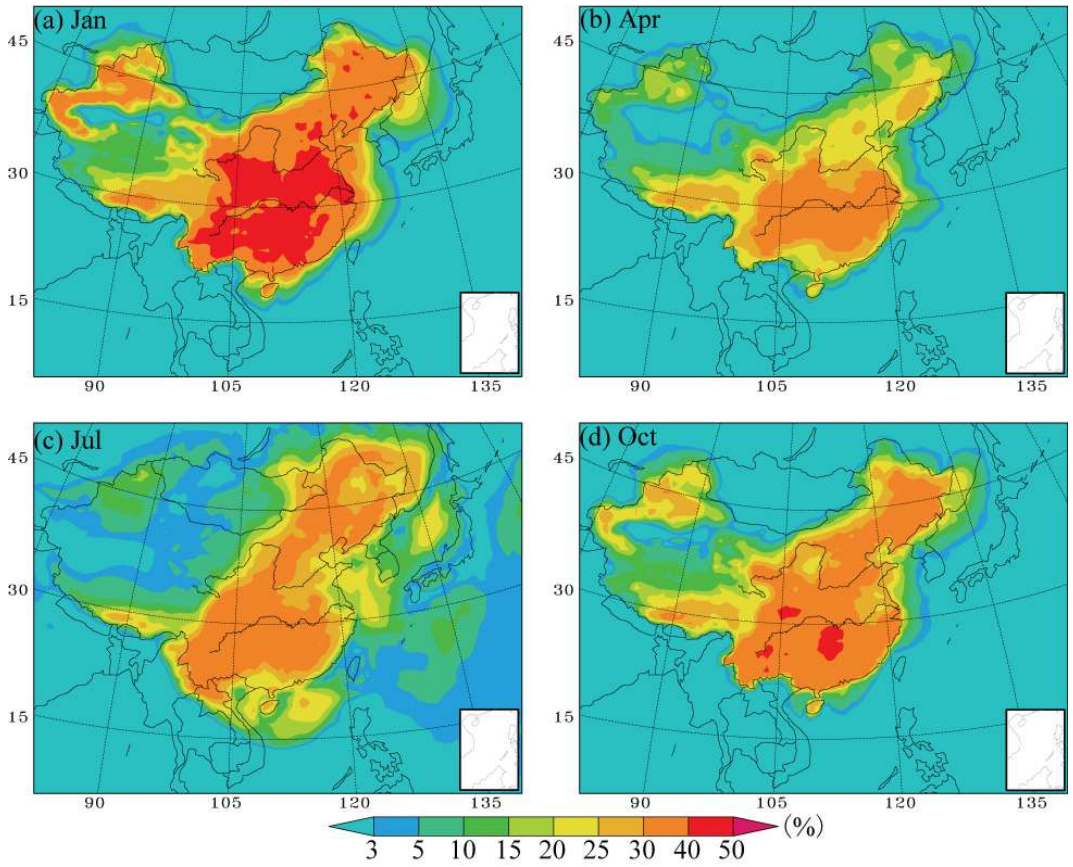

Figure 6. The horizontal distributions of the contribution percentage of NH_3 emissions to SNA mass concentration (%) in January, April, July and October.

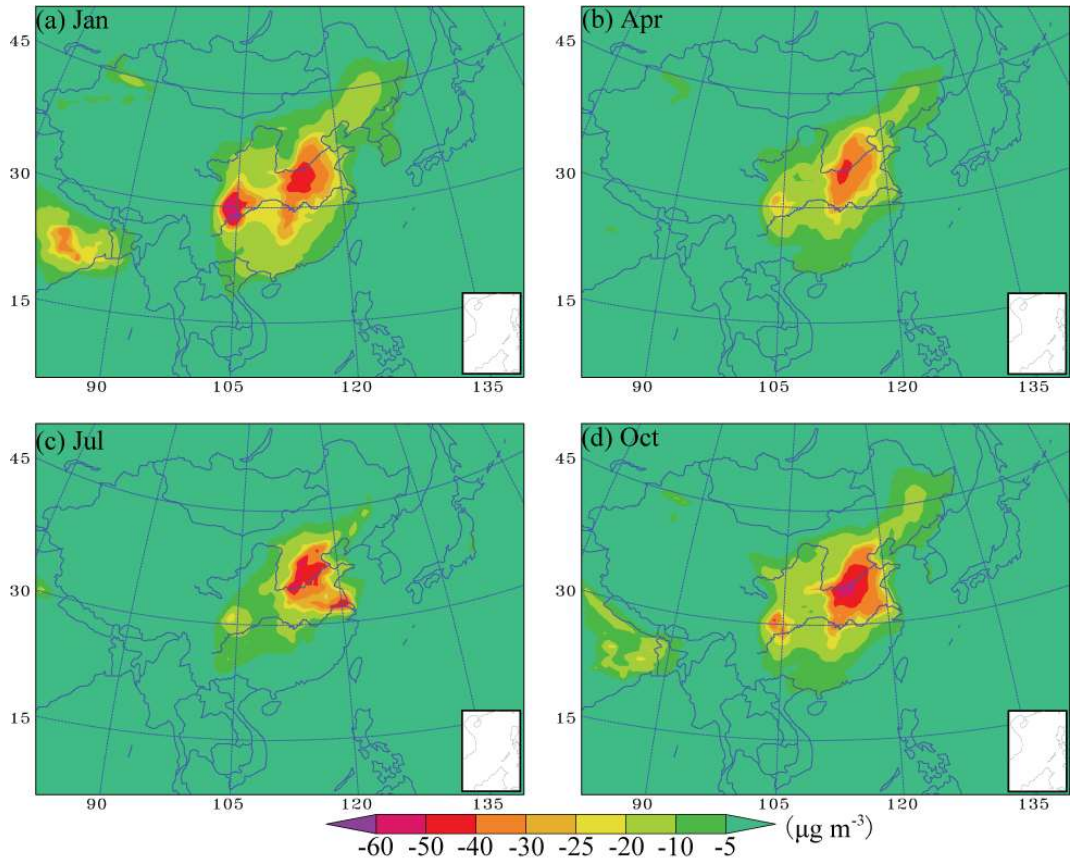

Figure 7. The horizontal distributions of SNA mass concentration (μg m^{-3}) variation associated with agriculture NH_3 removal in January, April, July and October.

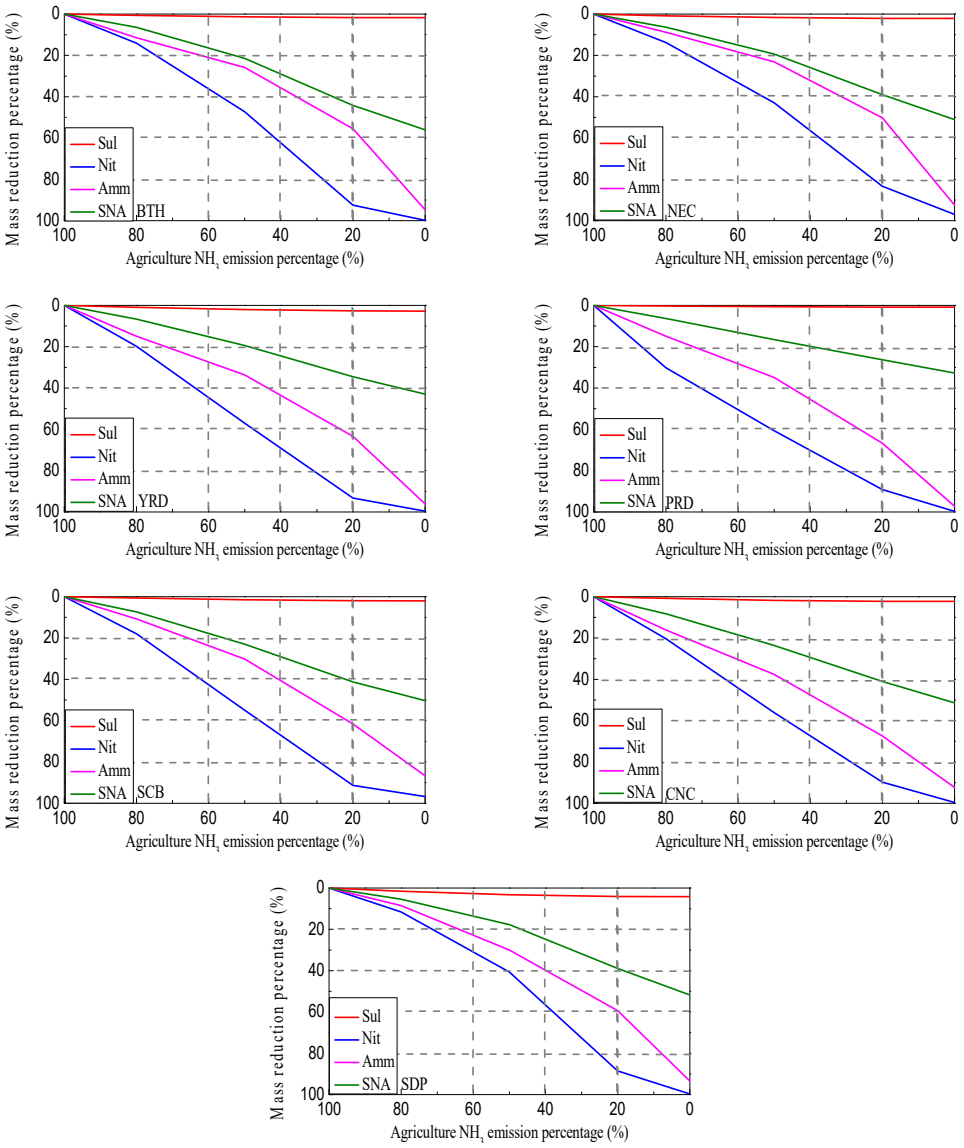

Figure 8. The variation (%) of sulfate, nitrate, ammonium, and SNA mass burden associated with the NH_3 emission reduction (%).

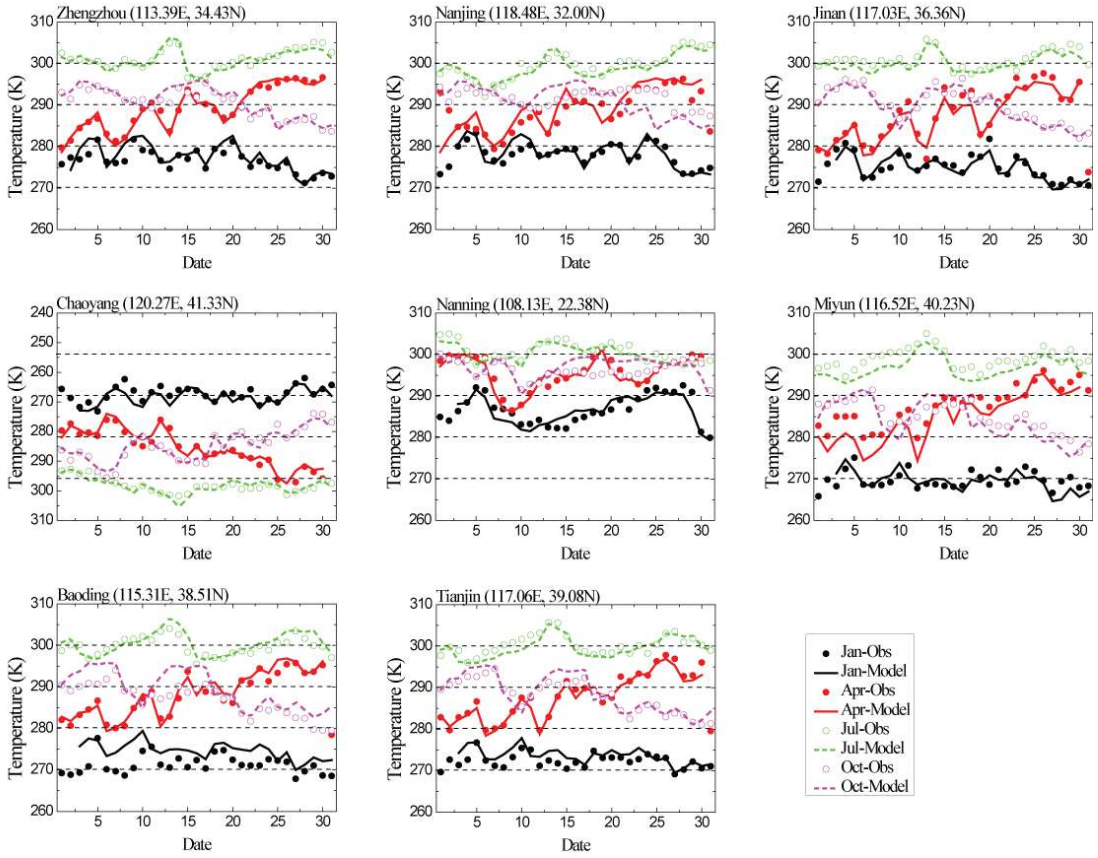

Figure A1. Observed and modeled daily average temperatures (K) in January, April, July and October 2015.

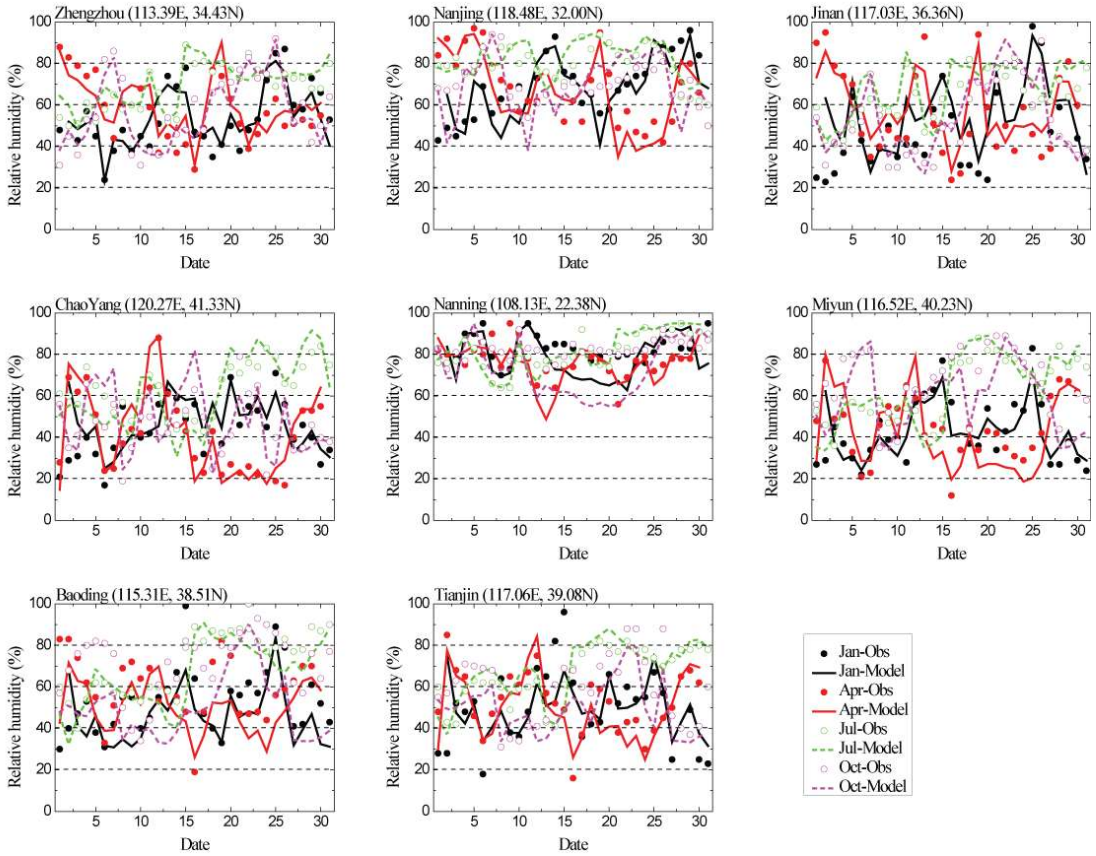

Figure A2. Same as Figure A1 but for relative humidity (%)

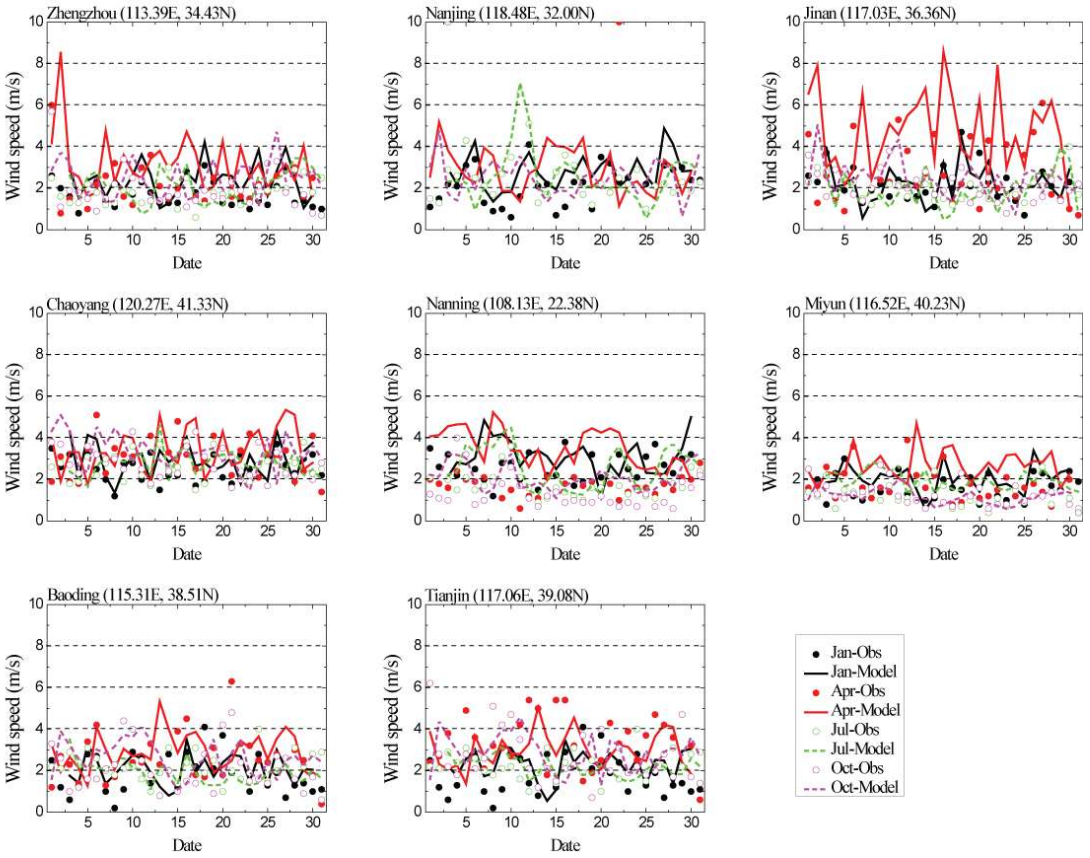

Figure A3. Same as Figure A1 but for wind speed (m s^{-1})

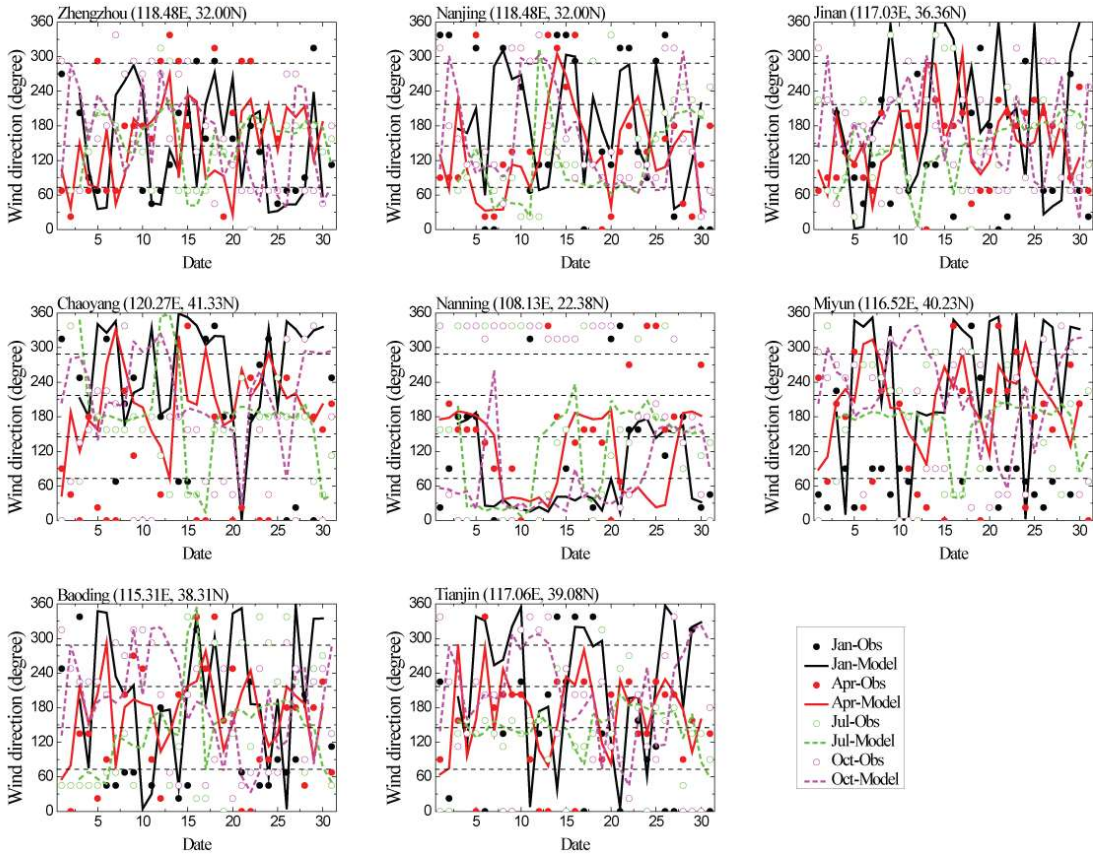

Figure A4. Same as Figure A1 but for daily maximum wind direction (degree)

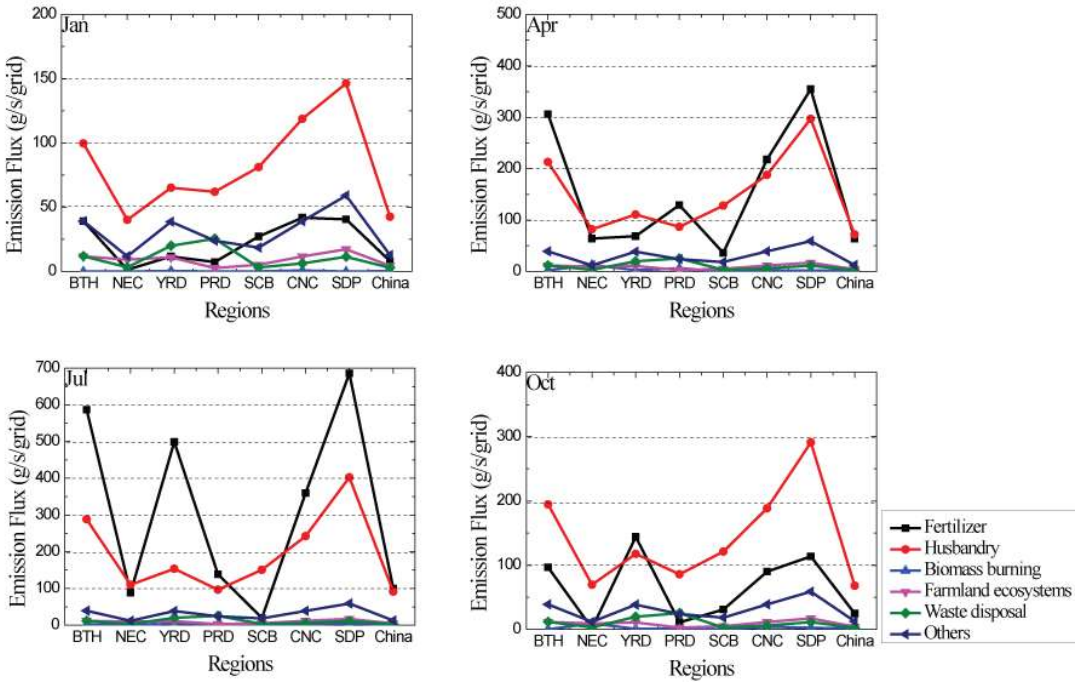

Figure A5. The regional average NH_3 emission flux (g/s/grid) of different agriculture sectors over each region in January, April, July and October.

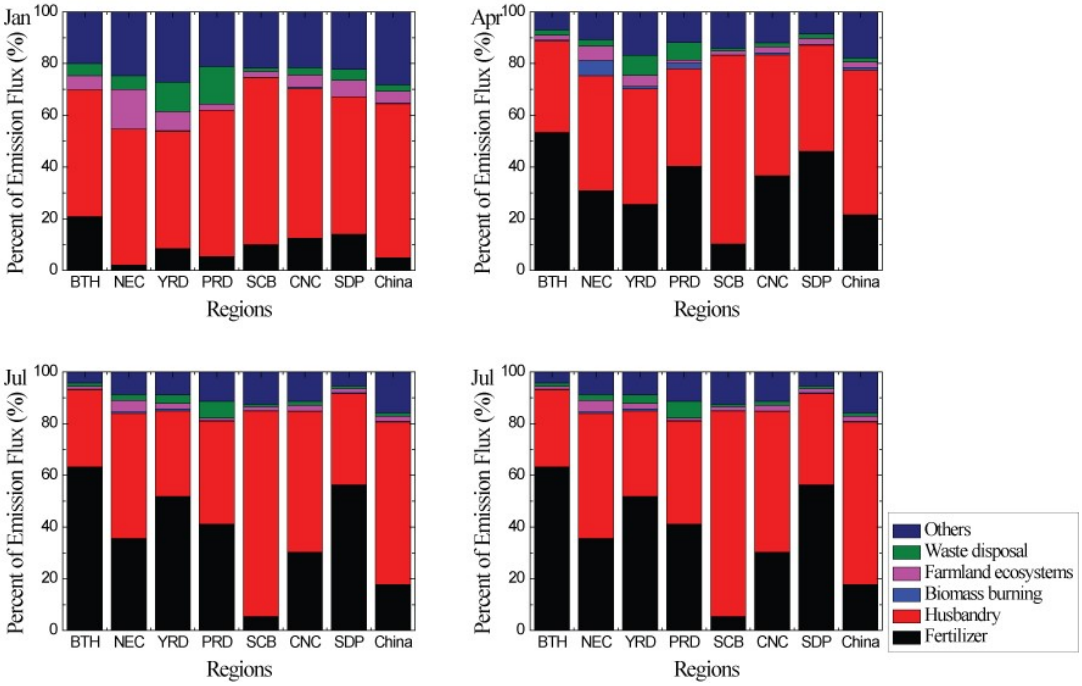

Figure A6. The percent (%) of different NH_3 emission sectors over each region in January, April, July and October.

Table 1. Statistical summary of the comparisons of the monthly average $PM_{2.5}$ between simulation and observation

	N^a	O^b	M^c	$\sigma_o{}^d$	$\sigma_m{}^e$	R^f
Jan	4464	106.5	126.9	84.5	76.2	0.74
Apr	4320	64.6	76.8	44.7	56.8	0.66
Jul	4464	49.2	42.1	32.3	41.4	0.58
Oct	4464	58.2	68.1	35.5	46.9	0.61

[a] Number of samples

[b] Total mean of observation

[c] Total mean of simulation

[d] Standard deviation of observation

[e] Standard deviation of simulation

[f] Correlation coefficient between daily observation and simulation

Table 2. Statistical summary of the comparisons of the monthly average NO_2 between simulation and observation

	N	O	M	σ_o	σ_m	R
Jan	4464	79.7	87.1	39.8	39.0	0.60
Apr	4320	53.7	55.5	29.9	32.5	0.59
Jul	4464	43.6	40.1	25.8	30.0	0.51
Oct	4464	53.6	61.3	32.0	31.7	0.54

Table 3. Statistical summary of the comparisons of the monthly average SO_2 between simulation and observation

	N	O	M	σ_o	σ_m	R
Jan	4464	61.0	71.5	61.3	47.5	0.63
Apr	4320	24.8	35.7	26.5	24.6	0.52
Jul	4464	13.9	22.4	15.1	19.1	0.46
Oct	4464	21.2	36.8	20.2	21.8	0.50

Table 4. The regional percent (%) of Tagr NH_3 contribution to sulfate, nitrate, ammonium, and SNA mass concentration.

		Sulfate	Nitrate	Ammonium	SNA	$PM_{2.5}$
BTH	Jan	0.9	4.5	98.0	39.7	19.3
	Jul	1.0	9.3	75.9	28.1	20.6
	Annual	1.1	8.0	83.3	23.1	15.5
NEC	Jan	0.6	3.2	94.0	34.4	18.6
	Jul	0.8	6.7	83.5	27.9	16.1
	Annual	1.0	5.6	83.7	22.5	14.3
YRD	Jan	0.9	5.8	99.2	40.9	22.5
	Jul	0.5	8.1	68.7	24.0	15.4
	Annual	1.0	7.4	85.7	23.6	15.3
PRD	Jan	0.8	5.0	98.1	40.2	20.4
	Jul	1.4	4.7	85.3	27.7	15.9
	Annual	0.9	5.8	90.6	24.5	14.2
SCB	Jan	0.6	3.7	97.0	37.4	17.9
	Jul	0.7	5.6	95.9	31.5	19.5
	Annual	0.7	5.1	93.9	21.6	13.0
CNC	Jan	0.9	4.9	99.2	42.6	20.6
	Jul	0.9	6.7	88.9	33.7	22.0
	Annual	0.9	6.0	92.8	26.1	17.5
SDP	Jan	0.7	4.9	98.3	39.2	21.0
	Jul	0.7	8.3	67.0	23.5	16.6
	Annual	0.9	7.1	80.5	21.6	15.1
China	Jan	2.4	9.3	92.3	34.4	21.4
	Jul	2.2	10.4	90.9	25.1	16.4
	Annual	2.2	10.1	87.6	29.0	16.0

998 Table 5. The variation percent (%) of sulfate, nitrate, ammonium, and SNA mass concentration associated with
999 agriculture NH_3 removal.

		Sulfate	Nitrate	Ammonium	SNA	$PM_{2.5}$
BTH	Jan	0.5	99.8	96.2	51.9	37.8
	Jul	1.0	99.6	95.0	47.0	39.2
	Annual	0.7	99.8	94.7	49.4	38.5
NEC	Jan	0.7	99.2	96.4	60.9	39.2
	Jul	0.8	94.5	91.5	37.0	27.8
	Annual	0.7	96.9	92.5	48.9	34.5
YRD	Jan	2.7	99.4	96.0	52.6	32.2
	Jul	7.2	99.0	96.8	44.9	37.6
	Annual	5.0	99.2	96.1	48.8	36.9
PRD	Jan	3.6	99.8	97.2	50.3	31.5
	Jul	0.4	92.7	97.4	30.3	24.1
	Annual	2.0	96.2	97.2	40.3	27.8
SCB	Jan	4.9	94.1	80.3	57.6	41.7
	Jul	0.2	99.3	92.5	42.0	28.3
	Annual	2.6	96.7	85.9	49.8	35.0
CNC	Jan	3.1	99.1	92.2	56.7	41.5
	Jul	0.7	99.3	96.0	45.1	37.2
	Annual	1.9	99.2	92.3	50.9	39.4
SDP	Jan	1.7	99.8	95.8	47.7	38.0
	Jul	3.6	99.2	93.6	45.6	37.3
	Annual	2.7	99.5	93.4	46.6	37.6
China	Jan	2.6	93.9	86.3	54.8	39.5
	Jul	0.6	97.7	87.8	36.7	27.5
	Annual	1.6	95.8	86.9	45.7	32.9

1000
1001
1002
1003
1004